Title
An atomistic view of structural and electronic properties of rare earth ensembles on Si(001) substrates

Journal
Chemical Physics Letters, 466(4-6)

ISSN
0009-2614

Authors
Shinde, Aniketa
Cao, Juexian
Lee, Sangyeob
et al.

Publication Date
2008-12-01

DOI
10.1016/j.cplett.2008.10.040

Chemical Physics Letters 466 (2008) 159–164

Contents lists available at ScienceDirect

Chemical Physics Letters

journal homepage: www.elsevier.com/locate/cplett

An atomistic view of structural and electronic properties of rare earth ensembles on Si(001) substrates

Aniketa Shinde [a,b], Juexian Cao [a], Sangyeob Lee [b], Ruqian Wu [a], Regina Ragan [b,*]

[a] Department of Physics and Astronomy, University of California, Irvine, California 92697-4575, USA
[b] Department of Chemical Engineering and Materials Science, University of California, Irvine, California 92697-2575, USA

ARTICLE INFO

Article history:
Received 23 August 2008
In final form 14 October 2008
Available online 18 October 2008

ABSTRACT

Synergistic experimental and theoretical studies of low coverage adsorption geometries of rare earth adatoms on Si(001) were performed. Density functional calculations showed charge transfer from adatoms to Si(001) and explained observed bias dependence in scanning tunneling microscopy images. Comparison of STM simulations with empty states STM data revealed a direct correlation between coverage and surface reconstructions; the (4×8) reconstruction is a low coverage precursor to (2×4) reconstruction. Charge transfer from adatom to substrate was also confirmed by Kelvin probe force microscopy; contact potential difference measurements of Dy/Si(001) reveal a 0.28 eV higher surface potential than that of (2×1) reconstructed Si.

1. Introduction

Rare earth disilicide ($RESi_{2-x}$) nanowires self-assemble on Si(001) [1–4] from precursors consisting of rare earth adatoms on Si(001) surfaces. $RESi_{2-x}$ nanostructures have been a topic of considerable interest due to their high conductivity and low Schottky barrier on *n*-type silicon and thereby have potential for use as nanoscale interconnects [5]. Recently a related material system, YSi_2 nanowires on Si(001), has exhibited short-range charge ordering and Van Hove singularities that are exhibited in only one-dimensional metallic structures such as carbon nanotubes [6]. Since disilicide nanostructures are fabricated in ultrahigh vacuum conditions, pristine surfaces can be probed *in situ* in order to correlate morphology and electronic properties. Thus, disilicide nanostructures represent a model system to understand electronic properties in quantized metallic structures. Furthermore, $RESi_{2-x}$ may also be used as templates for self-organization of coinage metals into nanoparticle and nanowire arrays that otherwise would not readily form as stable monodisperse nanostructures on Si substrates [7]. These bimetallic nanostructures may have tunable chemical activity as a function of size, shape and material interfaces, suitable for broad applications [8].

The formation of disilicide nanowires on Si(001) is governed by the asymmetric strain between $RESi_{2-x}$ in the hexagonal aluminum diboride (AlB_2) type lattice and the Si(001) diamond cubic lattice [9]. Yet the complex surface reconstructions that lead to nanowire nucleation perpendicular to Si dimer rows on (2×1) reconstructed surfaces has not been clearly elucidated. In order to further control the growth morphology and utilize physical properties of $RESi_{2-x}$ nanostructures, it is crucial to understand the interaction between RE adatoms and the Si substrate. Thus, we have performed first principles calculations based on the density functional theory (DFT) and compared theoretical results with experimental scanning probe microscopy (SPM) data of $RESi_{2-x}$ (RE = Er, Dy) precursor structures. Since scanning tunneling microscopy (STM) images typically exhibit a strong bias dependence [10–13], simulated STM images provide a means for correct interpretation of surface atomic structure. In order to circumvent the problem dealing with the strongly localized 4f shell, we used yttrium to represent RE elements in our ab initio calculations. Y is a trivalent atom that does not have f valence electrons but has chemical and physical properties very similar to the RE elements [14–16]. The omitted 4f shell is essential for magnetic properties but should not affect their bonds with Si for the discussion below.

In our previous work, a preferred binding site for Y on Si(001) was identified as having a binding energy 400 meV lower than other metastable binding sites [13]. In this Letter, the simulated STM images and charge density difference profiles of Y adatoms in the preferred binding site on Si(001) are compared with experimental results of STM images and Kelvin probe force microscopy (KPFM) analysis. This work provides insight into atomic structure, thermodynamic forces guiding assembly and surface electronic structure of the RE/Si(001) system.

2. Experimental details

Si (2×1) reconstructed surfaces were prepared by flashing samples at 1150 °C for 30 s with a pressure less than 5×10^{-10} Torr, then cooled down quickly to 900 °C and held for

* Corresponding author. Fax: +1 949 824 2541.
E-mail address: rragan@uci.edu (R. Ragan).

0009-2614/$ - see front matter © 2008 Elsevier B.V. All rights reserved.
doi:10.1016/j.cplett.2008.10.040

1 minute. The samples were then cooled down slowly to room temperature and the (2×1) reconstruction was verified with STM. Dysprosium or erbium were evaporated from a molybdenum crucible onto *p*-type (dopant density $n = 10^{18}$–8×10^{18} cm^{-3}) nominally flat and 2.5° miscut Si(001) substrates ($n = 7 \times 10^{17}$ cm^{-3}). The samples were heated to approximately 600 °C and RE was deposited using an *in situ* Mantis mini E-beam evaporator. Post annealing was done at 600 °C or 680 °C for 2 min. STM and KPFM were conducted in an ultra high vacuum Omicron variable temperature STM and atomic force microscope (AFM) system attached to the deposition system for surface analysis without exposure to ambient conditions. All STM images were acquired at room temperature under constant current mode.

Frequency modulated KPFM, as demonstrated by Kitamura and Iwatsuki et al. [17,18], was performed at room temperature with super sharp silicon tips (Nanosensors SSS-NCHR) having a typical radius of curvature of 2 nm. An additional 3 nm of Cr was deposited onto the AFM tip side to ensure the conducting layer needed for KPFM data acquisition. The cantilever was oscillated at the resonant frequency of 270 kHz and with a constant amplitude of approximately 7 nm [19]; contact potential difference (V_{CPD}) measurements were obtained with 2 kHz and 2.0 $V_{peak-peak}$ applied AC voltage. KPFM has the capability to simultaneously image topography and V_{CPD} between the surface and the probe with atomic resolution. V_{CPD} is defined in the following equation when the bias is applied to the tip [20]:

$$eV_{CPD} = \Phi_{tip} - \Phi_{sample} \quad (1)$$

where Φ_{tip} and Φ_{sample} are the work function of the tip and the sample, respectively, and e is the electron charge. Thus, an increase in V_{CPD} corresponds to a lower work function of the sample when the same tip is used. Using this scanning probe based technique, work function variations across different nanostructures on surfaces can be resolved [17]. In comparison, photoemission spectroscopy also measures work function but it is not possible to correlate surface morphology with nanometer resolution since the typical beam size is on the order of a few 100 μm [21]. When KPFM results are compared with photoemission data for thin films and adsorbates, the trends of measured work function values are in good agreement [22,23].

3. Computational approaches

First principles calculations were performed within the density-functional framework using the generalized gradient approximation (GGA) for the exchange correlation energy functional (PW 91), as implemented in the Vienna *ab initio* Simulation package (VASP) [24]. Ultra-soft pseudopotentials (US PP) [25] and a plane-wave basis set with energy cutoff of 350 eV were used. The Si(001) surface is modeled by periodically repeating slabs made up of six layers of Si(001) and 15 Å of vacuum. In the lateral plane, we adopted a (3×4) supercell to mimic the low adsorption environment. The $2 \times 2 \times 1$ *k*-points were used to sample the Brillouin zone. The top three layers of Si along with the adatoms were allowed to relax, with a criterion that forces are lower than 0.01 eV/Å. The bottom three layers of Si were fixed and dangling bonds were passivated with hydrogen atoms. The change in adsorption energies of a single Y adatom on a thicker Si(001) slab, 8- or 12-layers (4 or 6 relaxed layers), was less than the thermal energy for RE deposition on Si at 600 °C (75 meV).

4. Results and discussion

Fig. 1a is a typical STM image of $ErSi_{2-x}$ nanowires having Er coverage of approximately 0.1 monolayer (ML) on a vicinal Si(001) surface with a 2.5° miscut toward [110]. $RESi_{2-x}$ nanowires grow unidirectional, perpendicular to Si dimer rows, on vicinal Si(001)[3] and in two orthogonal directions on nominally flat Si(001) substrates [9]. The STM image of Fig. 1b shows a 30 nm × 30 nm region of a sample with Er coverage slightly less than 0.1 ML. Distinct periodicities, or surface reconstructions, can be seen on the Si(001) surface between $ErSi_{2-x}$ nanowires that result from various numbers of Er atoms in a group on the Si(001) surface. The bright features extending along the [110] direction are Si dimer rows; these dimer rows provide a reference for crystallographic orientation. Although $[1\bar{1}0]$ and [110] are indistinguishable directions in bulk Si, the symmetry is broken on the surface of a reconstructed Si(001) terrace due to dimer formation. In this paper, $[1\bar{1}0]$ refers to a direction perpendicular to dimer rows and [110] indicates the direction parallel to dimer rows on a terrace. The high resolution STM image of Fig. 1c acquired for the occupied states shows that along $[1\bar{1}0]$ the periodicity of the small bright features in the metal reconstructed region is the same as that of the dimer rows, 2×3.84 Å, or 2 a_{Si}. The Si dimers at the lower left corner of Fig. 1c, indicated by an arrow, provide a natural scale marker for a_{Si} along [110], where the zigzag pattern of the buckled dimer has a periodicity of 2 a_{Si}. Since the spacing between small dim features along [110] is also an integer value of a_{Si}, typically 2 or 3, one can conclude that the Er atoms form commensurate structures along [110] on the Si(001) substrate. However, it is difficult to resolve the adsorption site of metal atoms and the complex metal-induced surface reconstruction merely from the STM images.

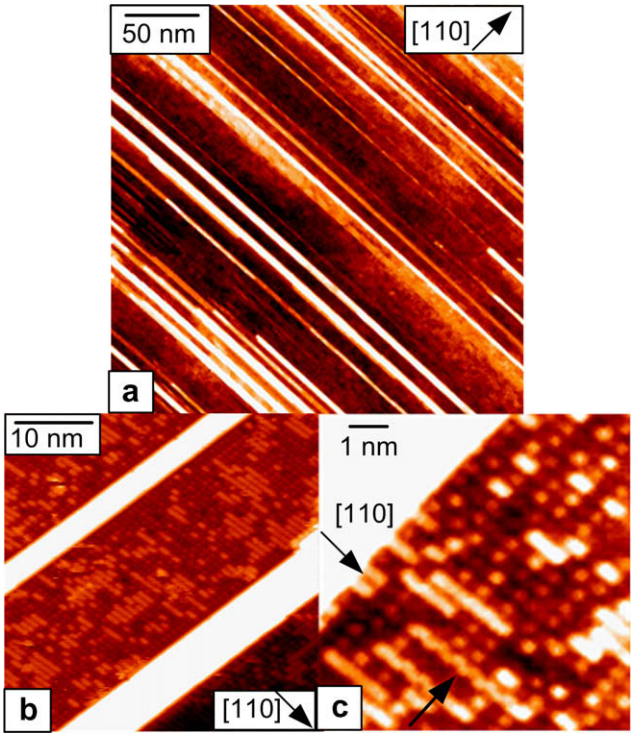

Fig. 1. STM images acquired with a feedback current of 100 pA of (a) a 250 nm × 250 nm region of $ErSi_{2-x}$ nanowires on a vicinal Si(001) substrate with a 2.5° miscut toward [110] at $V_{bias} = -1.9$ V, (b) a 30 nm × 30 nm region of $ErSi_{2-x}$ nanowires on a nominally flat Si(001) substrate at $V_{bias} = -1.9$ V and (c) a 10 nm × 10 nm region at $V_{bias} = -2.1$ V. The bright intensity in the upper left hand corner of the image in (c) results from a nanowire. The arrow in the lower left corner points to buckled Si dimers on the surface with periodicity 2 a_{Si} in the [110] direction.

To identify the location of rare earth atoms, density functional simulations were performed for proper interpretation of experi-

mental STM data. The preferential binding site of Y on Si(001) was previously found to be located in a four-fold hollow site between Si dimer rows (*interrow*$_{dn}$) with a binding energy at least 400 meV lower in energy than other possible binding sites [13]. Utilizing this adsorption geometry, Fig. 2a and b show the simulated STM images of Y/Si(001) in a region of 0.15 nm × 0.12 nm for both the empty and occupied states, respectively. The position of the Y adatom, indicated by an 'x' in the images, switches between an intensity maximum and minimum with varying sample bias. Specifically, one bright maximum is observed on Y under empty states imaging conditions (+2.0 V sample bias). In contrast, four bright lobes are found on top of the position of Si atoms under occupied states imaging conditions (−2.0 V sample bias), as indicated by the small white circles in Fig. 2b, while the position marked with 'x' now appears as a dark spot. From the simulations one can easily conclude that the position of a Y adatom does not overlap with a bright feature in the occupied states STM images and furthermore, there is not always a direct correspondence between the number of bright spots and number of adatoms. The shift in the position of bright features between empty and occupied states is important for correct understanding of STM images of RE/Si(001).

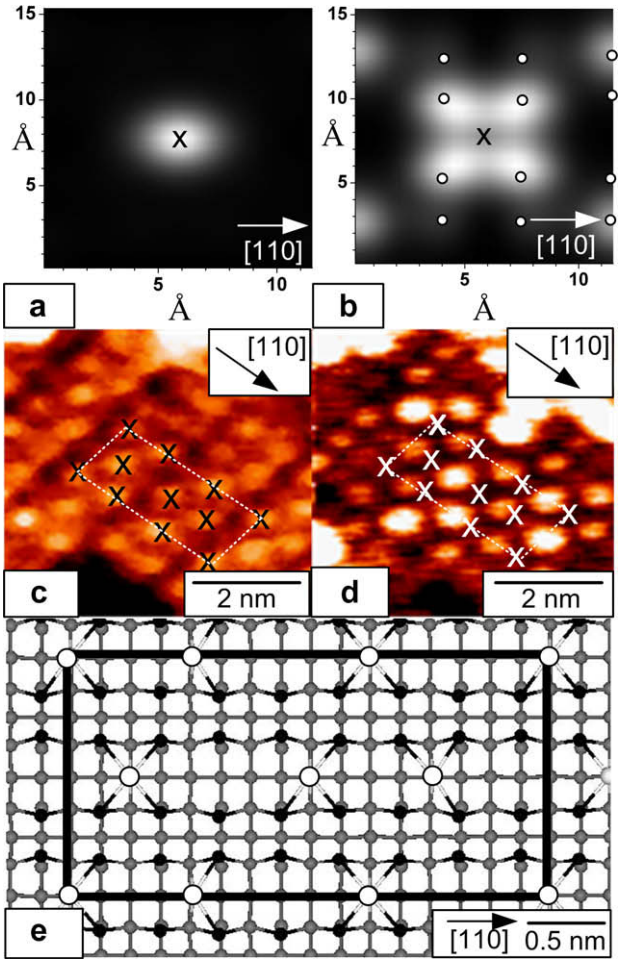

Fig. 2. A 0.15 nm × 0.12 nm simulated STM image for 1 Y adatom on Si(001) with (a) V_{bias} = +2.0 V and (b) V_{bias} = −2.0 V. The Y position is indicated by an 'x' and surface Si in dimer locations are indicated by small white circles in (b). STM images acquired with a feedback current of 100 pA of Er on a nominally flat Si(001) substrate of (c) a 5 nm × 5 nm region at V_{bias} = +2.0 V and corresponding filled states image (d) with V_{bias} = −2.1 V. The 'x' corresponds to the same positions in (c) and (d) and the white dashed rectangle outlines the (4 × 8) reconstruction. A ball and stick schematic (e) shows RE adatoms (white circles) each at the preferred binding site, surface Si (black circles), four bulk Si layers underneath (gray circles) and the black rectangle outlines the corresponding (4 × 8) unit cell.

The STM images in Fig. 2c and d are simultaneously acquired from the same area on the surface of an Er/Si(001) sample with a bias of +2.0 V in the backward scan for Fig. 2c and −2.1 V in the forward scan for Fig. 2d. An 'x' is located on intensity maxima during empty states imaging and marks the same locations in both Fig. 2c and d, presumably right on top of Er adatoms as concluded from the discussions above. In agreement with the simulation of Fig. 2b, the Er adatom position is surrounded by four bright protrusions for occupied states in Fig. 2d, demonstrating the bias dependence of surface reconstruction. The empty states image of Fig. 2c shows a (4 × 8) reconstruction that has not been reported previously whereas the occupied states image of Fig. 2d represents what has been reported as a $c(4 \times 2)$ reconstruction for Er on Si(001) [10]. The (4 × 8) reconstruction unit cell is outlined by a white dashed rectangle both in Fig. 2c and d. A ball and stick model is shown in Fig. 2e to illustrate the positions of RE adatoms (white circles), surface Si atoms (black circles) and subsurface Si (gray circles). The black rectangle outlines the corresponding (4 × 8) unit cell outlined in Fig. 2c and d.

STM images are not only bias dependant but coverage dependant as well [10,12]. Thus, stable geometries with multiple Y atoms on Si(001) were also investigated via first principles calculations. Six Y atoms were placed on a (4 × 4) unit cell so as to allow a large freedom for local reconstructions. The simulated STM image for the ground state structure is shown in Fig. 3a with a sample bias of +0.7 V from which one observes that Y adatoms form commensurate chains along the $[1\bar{1}0]$ direction. The calculated optimized structure resulting from the simulation is illustrated in the schematic of Fig. 3b and notably the presence of groups of Y atoms (white circles) opens Si dimers (black circles) nearby. During relaxation, the surface silicon atoms that were previously dimerized moved approximately 0.6 Å further apart. The periodicity and the elliptical shape of the central bright feature in the simulated image are also observed in experimental STM images under the same bias as shown in Fig. 3c. The white dashed rectangle on the right side of the image highlights groups of three protrusions along the [110] direction having the same unit cell as shown in the schematic of Fig. 3b. Because of the difference in the atomic environment around the three Y atoms, the brightness on top of the central Y atom is different from the edge Y atoms in both simulated and experimental data, shown in Fig. 3a and c respectively. This alternating intensity was also observed by Liu et al. for Dy on Si(001) at a bias of +0.46 V and has been identified as (2 × 4) reconstruction [12]. The alternating intensity was assigned as a result of buckling of Dy atoms, however our DFT calculations did not show any meaningful buckling of adatoms. Thus, the difference in brightness in the empty states image is purely due to electronic features rather than topography. It is interesting to further explore the coverage dependence of STM images and reconstructions by comparing the atomic arrangements in Fig. 3b with that in Fig. 2e. The (4 × 8) reconstruction has six RE adatoms per unit cell whereas Fig. 3b would have 12 RE adatoms for the same dimensions. The (2 × 4) reconstruction results if six additional adatoms are added to Fig. 2e in positions leading to the trimers seen in Fig. 3b. Thus, it can be inferred that the (4 × 8) reconstruction has half the RE coverage than that of the (2 × 4) reconstruction.

The good agreement between theoretical and experimental STM images establishes the reliability of the geometric models obtained through density functional calculations. We thus provide more electronic information that is hard to obtain through experimental means. Charge transfer between Y and Si was explored by producing contours of charge density difference, $\rho_{Y/Si(001)} - \rho_{Si(001)} - \rho_{Y}$, that are shown in Fig. 4. From the cross section it is clear that charge leaves the Y adatom (blue contour lines) and accumulates in the region between Y and the subsurface Si atoms (pink contour lines), a trend that is in good accordance with electronegativities

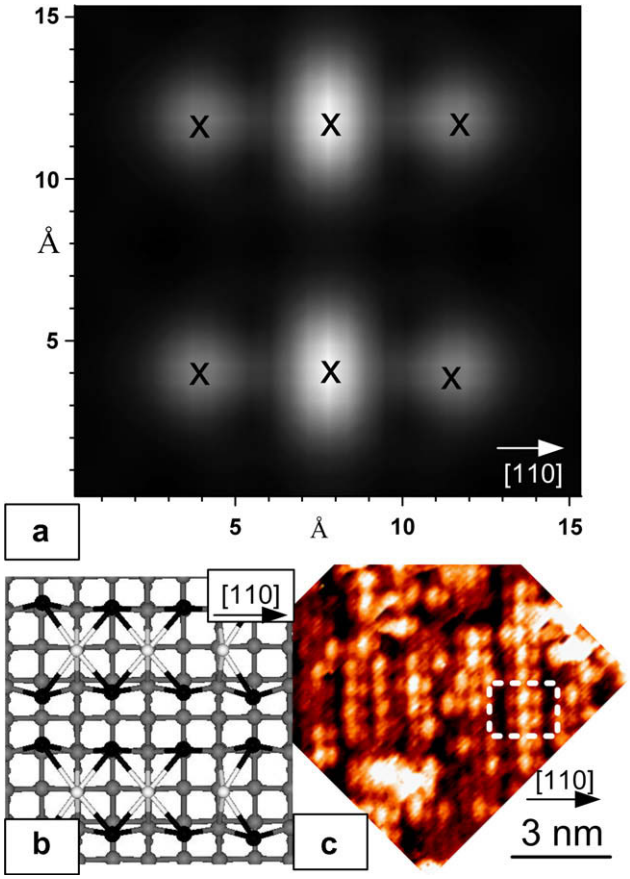

Fig. 3. (a) Simulated STM image with V_{bias} = +0.7 V of 6 Y adatoms on Si(001) with the atomic positions indicated by an 'x', (b) calculated relaxed positions of the simulated image of (a) showing the 6 Y (white circles) adatoms each at the preferred binding site, surface Si atoms that were formerly dimers (black circles) and four layers of bulk Si underneath (gray circles). (c) The experimental STM data for Er/Si(001) was acquired with V_{bias} = +0.7 V and a tunneling current of 100 pA and shows groups of 3 maxima making a chain in the $[1\,\bar{1}\,0]$ direction similar to the simulation in (a) and (b). The dashed white rectangle in (c) highlights the grouping of adatoms seen in the unit cell in (a) and (b).

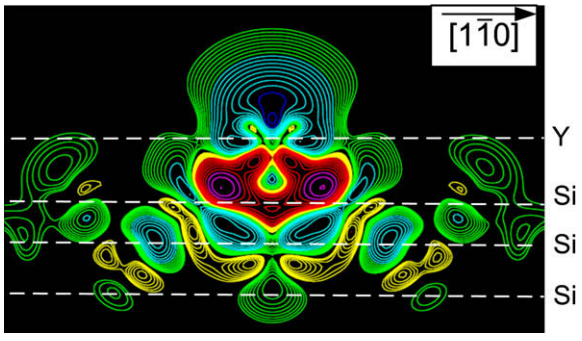

Fig. 4. Simulated charge density difference image for 1 Y adatom on Si(001) with the cross section along the $[1\,\bar{1}\,0]$ direction. Charge accumulation increases from yellow to pink contour lines whereas charge depletion increases from green to blue contour lines. The greatest charge depletion is seen at the Y adatom location and the greatest charge accumulation is seen in the region between Y and the subsurface Si atoms. Contours start from ± 0.001 e/Å^3 (yellow and green) where e is the electron charge and change successively by a factor of $\sqrt{2}$. (For interpretation of the references to colour in this figure legend, the reader is referred to the web version of this article.)

[26]. This charge transfer is expected to reduce the local work function as found for molecule/p-type Si(001) interfaces [22] and for surface defects on GaAs and GaP [27].

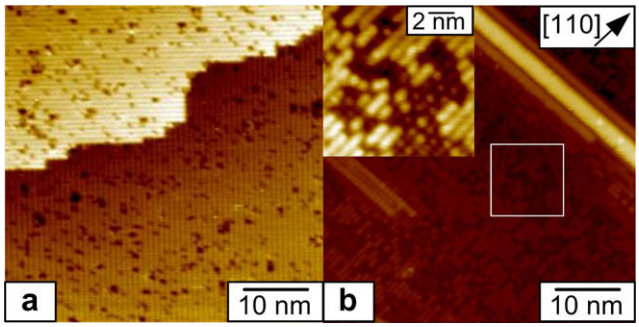

Fig. 5. 50 nm × 50 nm STM image of (a) a clean Si(001) (2 × 1) reconstructed surface taken at V_{bias} = −3.0 V and feedback current of 200 pA and (b) a Dy/Si(001) sample showing $DySi_{2-x}$ nanowires at V_{bias} = −2.0 V and feedback current of 300 pA. The inset shows Si dimer rows and Dy induced surface reconstruction in a 10 nm × 10 nm region as indicated by the white square.

In order to measure the effect of RE adatoms on the surface potential of Si(001), Dy was deposited on Si(001) with submonolayer coverage for subsequent KPFM analysis. V_{CPD} as a function of position on the surface is measured during KPFM imaging and represents the difference in work function between a conductive AFM tip and metallic sample as defined prior in Eq. (1). We will refer to the surface potential of clean silicon and RE induced reconstructed areas rather than work function since the silicon substrate is not metallic. Before Dy deposition, STM images verified a clean Si (2 × 1) reconstructed surface as seen in Fig. 5a. The V_{CPD} between the tip and clean (2 × 1) reconstructed Si(001) was measured as −0.91 ± 0.09 eV and will be used as a reference. After deposition of Dy on Si(001) with submonolayer coverage, KPFM analysis was performed on $DySi_{2-x}$ nanowires and regions surrounding $DySi_{2-x}$ nanowires and is shown in the V_{CPD} data of Fig. 6a and b after post-growth annealing at 600 °C and 680 °C, respectively. The energy scales are similar in both images and visually one can see that the V_{CPD} of areas between nanowires decreases (surface potential decreases) with the higher annealing temperature. A histogram of measured V_{CPD} values is shown in Fig. 7 where the mean values ± full width half maximum are −0.63 ± 0.09 eV for the sample post-annealed at 600 °C (gray squares), −0.79 ± .09 eV for the sample annealed at 680 °C post growth (open circles), and as mentioned prior −0.91 ± 0.09 eV for clean (2 × 1) reconstructed Si(001) (black squares). Thus, Dy induced reconstructed regions on the sample annealed at 600 °C have a larger V_{CPD} than the (2 × 1) reconstructed Si substrate, corresponding to a higher surface potential of 0.28 eV. The higher surface potential measured by KPFM confirms the presence of RE adatom induced surface dipoles as predicted by the density functional simulations. For the sample annealed at 600 °C, STM imaging verified the presence of areas of Si dimer rows coinciding with regions of Dy induced reconstruction in between $DySi_{2-x}$ nanowires similar to what is observed in Fig. 5b and its inset and the inset in Fig. 6a. STM data for the sample post-annealed at 680 °C (see Supplementary materials Fig. S1) reveal that the regions between nanowires have a dramatic decrease in Dy adatom coverage, leading to areas between $DySi_{2-x}$ nanostructures consisting of nearly 100% Si dimer rows, as seen in the inset of Fig. 6b. It is known that higher post-annealing temperatures of RE/Si(001) leads to nucleation of island structures and nanowires [28], indicating that unreacted adatoms may incorporate into disilicide nanostructures leaving (2 × 1) Si reconstructed areas between nanostructures. The decrease in adatom coverage does indeed result in a decrease of the mean V_{CPD} value toward that of (2 × 1) reconstructed Si; the difference between the sample annealed at 680 °C and Si(001) is 0.12 eV. The overall trend shows that as Dy adatom coverage increases, the surface potential in-

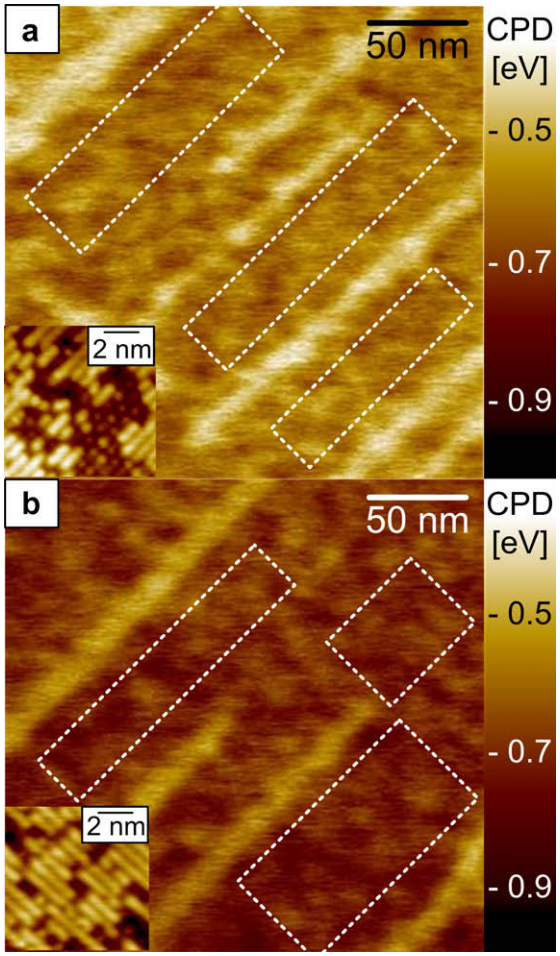

Fig. 6. 250 nm × 250 nm KPFM V_{CPD} images for $DySi_{2-x}$ nanowires and reconstructed regions between nanowires on Si(001) for samples annealed post-growth at (a) 600 °C and (b) 680 °C. Regions outlined by the dashed white rectangles are used to calculate the statistical values shown in the histogram displayed in Fig. 7. The 10 nm × 10 nm insets included are high resolution STM images representative of the Dy induced reconstruction present in the dashed white rectangles for each post-annealing temperature: more complete Si dimer reconstruction is seen in the inset of (b) than in (a), confirming the effects of higher temperature post-growth annealing.

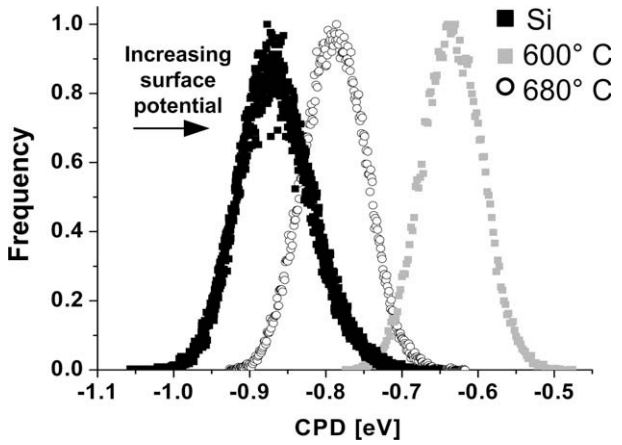

Fig. 7. Histogram of V_{CPD} values taken from a clean (2 × 1) reconstructed Si surface (black squares), a Dy/Si(001) sample post-annealed at 600 °C (gray squares) and a Dy/Si(001) sample post-annealed at 680 °C (open circles). The mean values ± full width half maximum are −0.91 ± 0.090 eV, −0.63 ± 0.09 eV and −0.79 ± 0.09 eV, respectively.

creases due to the presence of surface dipoles induced by the charge transfer between Dy adatoms and the silicon substrate, as predicted by the theoretical simulations.

5. Conclusions

Through combined a*b initio* calculations and SPM measurements, we studied the atomic structures and bonding mechanism for rare earth adatoms on Si(001). Y adatoms prefer the four-fold hollow sites and form linear trimers at higher coverage. With the aid of STM simulations to interpret experimental data, we found that six RE adatoms make up the (4 × 8) reconstruction unit cell, and doubling that coverage to twelve RE adatoms leads to the previously observed (2 × 4) reconstructions of RE on Si(001). Thus surface reconstruction and coverage were clearly correlated. Calculated charge transfer from adatoms to the silicon surface also predicts a decrease in the local work function, which was confirmed by measured V_{CPD} values in KPFM analysis. An increase in adatom coverage resulted in a corresponding increase in V_{CPD} (increase in surface potential) in comparison with that of (2 × 1) reconstructed Si. The correct interpretation of STM images of these complex systems provides a basis for further understanding of nucleation of $RESi_{2-x}$ nanowires on Si(001).

Acknowledgements

A.S. and R.R. thank S. Sadewasser for informative discussions about KPFM analysis. Acknowledgment is made to the Donors of the American Chemical Society Petroleum Research Fund for partial support of this research and National Science Foundation CBET-0731349 & CBET-0642217. RW also acknowledges support from DOE-BES DE-FG02-04ER15611. Calculations were performed on NERSC supercomputers.

Appendix A. Supplementary material

Supplementary material associated with this article can be found, in the online version, at doi:10.1016/j.cplett.2008.10.040.

References

[1] C. Preinesberger, S. Vandre, T. Kalka, M. Dahne-Prietsch, J. Phys. D Appl. Phys. 31 (1998) L43.
[2] B.Z. Liu, J. Nogami, Nanotechnology 14 (2003) 873.
[3] R. Ragan, Y. Chen, D.A.A. Ohlberg, G. Medeiros-Ribeiro, R.S. Williams, J. Cryst. Growth 251 (2003) 657.
[4] Y. Chen, D.A.A. Ohlberg, R.S. Williams, J. Appl. Phys. 91 (2002) 3213.
[5] K.N. Tu, R.D. Thompson, B.Y. Tsaur, Appl. Phys. Lett. 38 (1981) 626.
[6] C. Zeng, P.R.C. Kent, T. Kim, A. Li, H.H. Weitering, Nat. Mater. 7 (2008) 539.
[7] J.P. You, J.H. Choi, S. Kim, X.M. Li, R.S. Williams, R. Ragan, Nano. Lett. 6 (2006) 1858.
[8] C. Jo, J. Cao, A. Shinde, R. Ragan, R. Wu, Chem. Phys. Lett. 454 (2008) 327.
[9] Y. Chen, D.A.A. Ohlberg, G. Medeiros-Ribeiro, Y.A. Chang, R.S. Williams, Appl. Phys. Lett. 76 (2000) 4004.
[10] J.S. Yang, Q. Cai, X.D. Wang, R. Koch, Surf. Sci. 526 (2003) 291.
[11] C. Preinesberger et al., Appl. Phys. Lett. 87 (2005).
[12] B.Z. Liu, J. Nogami, Surf. Sci. 488 (2001) 399.
[13] A. Shinde, J. Cao, R. Wu, R. Ragan, Israel J. Chem. 48 (2008).
[14] L. Magaud, J.Y. Veuillen, D. Lollman, T.A.N. Tan, D.A. Papaconstantopoulos, M.J. Mehl, Phys. Rev. B 46 (1992) 1299.
[15] C. Rogero, C. Koitzsch, M.E. Gonzalez, P. Aebi, J. Cerda, J.A. Martin-Gago, Phys. Rev. B 69 (2004).
[16] C. Rogero, C. Polop, L. Magaud, J.L. Sacedon, P.L. de Andres, J.A. Martin-Gago, Phys. Rev. B 66 (2002).
[17] S. Kitamura, M. Iwatsuki, Appl. Phys. Lett. 72 (1998) 3154.
[18] S. Kitamura, K. Suzuki, M. Iwatsuki, Appl. Surf. Sci. 140 (1999) 265.
[19] Calculated amplitude given the geometry of the AFM system using the following equation provided by Omicron Nanotechnology:

$$A_{phys} = \frac{2l_{CL}}{52}\frac{\tan(A_{PSD})}{I_{tot}}$$

A_{phys} : physical amplitude of the tip oscillation (nm)
l_{CL} : cantilever length (nm)
A_{PKD} : voltage of the position sensitive detector (PSD)
I_{tot} : total PSD intensity (V).

[20] R. Shikler, T. Meoded, N. Fried, B. Mishori, Y. Rosenwaks, J. Appl. Phys. 86 (1999) 107.
[21] W. Schattke, M.A.V. Hove, Solid-state Photoemission and Related Methods: Theory and Experiment, Wiley-VCH, 2003.
[22] T. He et al., J. Am. Chem. Soc. 130 (2008) 1699.
[23] W. Song, M. Yoshitake, Appl. Surf. Sci. 251 (2005) 14.
[24] G. Kresse, J. Furthmuller, Phys. Rev. B 54 (1996) 11169.
[25] G. Kresse, D. Joubert, Phys. Rev. B 59 (1999) 1758.
[26] W. Monch, Semiconductor Surfaces and Interfaces, Springer, New York, 2001.
[27] T. Glatzel, S. Sadewasser, R. Shikler, Y. Rosenwaks, M.C. Lux-Steiner, Mat. Sci. Eng. B – Solid 102 (2003) 138.
[28] Y. Zhu, W. Zhou, S.H. Wang, T. Ji, X.Y. Hou, Q. Cai, J. Appl. Phys. 100 (2006).